THE JOURNAL OF BIOLOGICAL CHEMISTRY VOL. 283, NO. 39, pp. 26805–26819, September 26, 2008

Mathematical Model of Nucleotide Regulation on Airway Epithelia

*IMPLICATIONS FOR AIRWAY HOMEOSTASIS**

Received for publication, February 25, 2008, and in revised form, June 23, 2008 Published, JBC Papers in Press, July 28, 2008, DOI 10.1074/jbc.M801516200

Peiying Zuo[‡1], Maryse Picher[§1], Seiko F. Okada[§], Eduardo R. Lazarowski[§], Brian Button[§], Richard C. Boucher[§2], and Timothy C. Elston[¶2,3]

From the [‡]Department of Mathematics, the [§]Cystic Fibrosis/Pulmonary Research and Treatment Center, and [¶]Department of Pharmacology and the UNC Virtual Lung Group, University of North Carolina, Chapel Hill, North Carolina 27599

In the airways, adenine nucleotides support a complex signaling network mediating host defenses. Released by the epithelium into the airway surface liquid (ASL) layer, they regulate mucus clearance through P2 (ATP) receptors, and following surface metabolism through P1 (adenosine; Ado) receptors. The complexity of ASL nucleotide regulation provides an ideal subject for biochemical network modeling. A mathematical model was developed to integrate nucleotide release, the ectoenzymes supporting the dephosphorylation of ATP into Ado, Ado deamination into inosine (Ino), and nucleoside uptake. The model also includes ecto-adenylate kinase activity and feed-forward inhibition of Ado production by ATP and ADP. The parameters were optimized by fitting the model to experimental data for the steady-state and transient concentration profiles generated by adding ATP to polarized primary cultures of human bronchial epithelial (HBE) cells. The model captures major aspects of ATP and Ado regulation, including their >4-fold increase in concentration induced by mechanical stress mimicking normal breathing. The model also confirmed the independence of steady-state nucleotide concentrations on the ASL volume, an important regulator of airway clearance. An interactive approach between simulations and assays revealed that feed-forward inhibition is mediated by selective inhibition of ecto-5′-nucleotidase. Importantly, the model identifies ecto-adenylate kinase as a key regulator of ASL ATP and proposes novel strategies for the treatment of airway diseases characterized by impaired nucleotide-mediated clearance. These new insights into the biochemical processes supporting ASL nucleotide regulation illustrate the potential of this mathematical model for fundamental and clinical research.

Mucociliary clearance (MCC)[4] constitutes the first line of defense against airway infection (1). Inhaled pathogens are trapped by a mucus layer, positioned above ciliated epithelia by a periciliary (PCL) layer. Together, mucus and PCL form the ASL layer, which is continuously transported cephalad by coordinated ciliary beating. Through their interactions with P2 receptors, adenine nucleotides regulate all major epithelial functions supporting MCC, including Cl^-/liquid secretion via the Ca^{2+}-activated Cl^- channel and the cystic fibrosis transmembrane regulator (CFTR) (2), mucin secretion (3, 4), and ciliary beat activity (5, 6). Nucleotides are released by the epithelium into the ASL layer under basal conditions (7, 8), and their release rate increases in response to mechanical stress imparted by tidal breathing (8–12). Nucleotide-mediated epithelial responses are modified by surface enzymes (ectonucleotidases) that convert a fraction of the ATP into Ado (13–15). This nucleoside activates airway epithelial signaling pathways through P1 receptors, typically the A_{2B} receptor, which stimulates ciliary beat activity (16) and Cl^-/liquid secretion by CFTR (17). In healthy airways, the purinergic regulation of MCC is mediated by both P1 and P2 receptor-mediated responses (10, 18). In chronic lung diseases, the accelerated metabolism of ATP (14) can lead to severe complications related to airway obstruction and inflammation (2, 19). The cystic fibrosis (CF) patients are particularly vulnerable to infection because of the sole dependence of MCC on P2 receptor-mediated signaling, reflecting the absence of the final effector for P1 signaling, *i.e.* functional CFTR. This information led to the current interest in aerosolized nucleotide analogs for the improvement of MCC (19).

* This work was supported, in whole or in part, by National Institutes of Health Grants PPG-P01-HL034332, P30 DK065988, SCOR 1-P50-HL060280, SCCOR 1-P50-HL084934, and R01-GM079271. This work was also supported by Cystic Fibrosis Foundation Grants BUTTON06G0, OKADA06I0, and PICHER07I0. The costs of publication of this article were defrayed in part by the payment of page charges. This article must therefore be hereby marked "*advertisement*" in accordance with 18 U.S.C. Section 1734 solely to indicate this fact.

[1] Both authors contributed equally to this work.
[2] Both senior authors contributed equally to this work.
[3] To whom correspondence should be addressed: Dept. of Pharmacology, University of North Carolina, Chapel Hill, NC 27599. Tel.: 919-962-8655; E-mail: telston@med.unc.edu.

[4] The abbreviations used are: MCC, mucociliary clearance; ADA1, adenosine deaminase 1; Ado, adenosine; ASL, airway surface liquid; CFTR, cystic fibrosis transmembrane regulator; CCS, cyclic compressive stress; CF, cystic fibrosis; CNT3, concentrative nucleoside transporter 3; ecto-5′-NT, ecto-5′-nucleotidase; ecto-AK, ecto-adenylate kinase; E-NTPDases, ecto-nucleoside triphosphate diphosphohydrolases; E-NPPs, ecto-nucleotide pyrophosphatase/phosphodiesterases; HDL, high density lipoprotein; highNSAP, high affinity NSAP activity; HPLC, high pressure liquid chromatography; Ino, inosine; j_{Ado}, rate of Ado uptake; j_{Ino}, rate of Ino uptake; J_{ADP}, rate of ADP release; J_{AMP}, rate of AMP release; J_{ATP}, rate of ATP release; lowNSAP, low affinity NSAP activity; NTPDase 1, nucleoside triphosphate diphosphohydrolase 1; NTPDase 3, nucleoside triphosphate diphosphohydrolase 3; NSAP, nonspecific alkaline phosphatase; PCL, periciliary liquid layer; HBE, human bronchial epithelial cell; Ap_5A, P^1,P^5-di(adenosine 5′)-pentaphosphate.

Despite the importance of purinergic signaling for airway defenses, it has not been possible, until recently, to develop a mathematical model of ASL nucleotide regulation because of the absence of quantitative information regarding ASL nucleotide and Ado levels, the rates of nucleotide release and Ado uptake, and the kinetic properties of the ectonucleotidases. In the past decade, extensive work has been conducted to characterize ATP release from the apical surface of HBE cells (7, 8, 10–12, 20, 21). Members of the three ecto-ATPase families (alkaline phosphatases, ecto-nucleoside triphosphate diphosphohydrolases (E-NTPDases), and nucleotide pyrophosphatase/phosphodiesterases (E-NPPs)) (22, 23) have been identified on HBE cells (13–15, 24–26), along with ecto-AK (2ADP ↔ ATP + AMP) (27, 28). Also, Ado levels are regulated on HBEs by a balance between the production rate (AMP → Ado) by ecto-5′-NT and NSAP (13) and the elimination rate by Ado deaminase 1 (ADA1; Ado → Ino) and cellular uptake by concentrative nucleoside transporter 3 (CNT3) (29).

Based on these findings, we developed a mathematical model of ASL nucleotide regulation. The kinetic coefficients were optimized by fitting the output of the model to experimental values of ASL nucleotide and Ado concentrations, nucleotide release rates (12, 20), ATP metabolism (13, 26, 28), and Ado uptake (29). The capacity of the model to reproduce the impact of physical parameters (ASL volume and mechanical stress) and functional interactions between network components was verified by biochemical assays on primary cultures of HBE cells. This study provides the first mathematical approach to the investigation of an important defense mechanism in human airways.

EXPERIMENTAL PROCEDURES

Cell Culture—Model validation was conducted on HBE cultures maintained at air-liquid interface, as described previously (30). The epithelial cells were obtained from healthy donors at the time of transplantation by the Tissue Culture Core of the Cystic Fibrosis Center (University of North Carolina) under the auspices of protocols approved by the Institutional Board of Review. They were isolated by protease digestion, seeded on 12-mm permeable supports (0.45 μm pores, T-Clear; Costar) coated with human type IV collagen, and kept in Ham's F-12-based medium supplemented with 5 $\mu g \cdot ml^{-1}$ transferrin, 30 nM triiodothyronine, 1 μM hydrocortisone, and 3.75 $\mu g \cdot ml^{-1}$ endothelial cell growth substance. The confluent cultures were maintained at air-liquid interface with medium on the basolateral side. After 4 weeks, they were composed of ciliated and secretory cells, with transepithelial electrical resistance $\geq$300 ohms/cm^2.

Cyclic Compressive Stress (CCS)—The HBE cultures were subjected to 1 h of CCS mimicking normal tidal breathing (20 cm of H_2O; 20 cycles/min) using a system enclosed in an incubator (37 °C; 5% CO_2) (10). Two pieces of tubing, each containing a high speed solenoid valve, were inserted into a conical silicon plug fitted to the top of the T-Clear, one connected to a pressurized chamber and the other connected to the incubator atmosphere. A microprocessor regulated the amplitude and frequency of the chamber pressure applied to the culture by controlling the open/closed state of the solenoid valves (10).

Biochemical Measurements of Steady-state Nucleotide Concentrations—The steady-state ASL ATP concentration was measured on HBE cultures by luminometry using soluble luciferase or a chimeric *Staphylococcus aureus* protein A-luciferase attached to the apical surface via keratan sulfate-specific antibodies (20). Steady-state concentrations of ATP, ADP, AMP, and Ado were determined on HBE cultures by ethenyl derivatization and fluorescence high pressure liquid chromatography (HPLC) (12).

Transient Nucleotide Concentration Profiles and Ectonucleotidase Activities—HBE cultures were preincubated 30 min (37 °C; 5% CO_2) in Krebs buffer (pH 7.5) (0.35 ml; bilateral). Then 0.1–1000 μM ATP was added to the apical surface to determine the transient concentration profile and initial rate of ATP hydrolysis by HPLC analysis of buffer samples collected over 60 min (14). The contribution of each ectoenzyme was calculated from paired assays conducted on the same culture wells before and after pretreatment with selective noncompetitive inhibitor(s). The kinetic parameters of NSAP for ATP and ADP were determined as described previously for AMP (13), but in the presence of 0.5 mM Ap_5A to inhibit ecto-AK (ATP + AMP ↔ 2ADP) (28). NSAP activity was calculated from the difference in linear rate of substrate hydrolysis measured before and after exposure to 10 mM levamisole, at each substrate concentration (0.1–1000 μM). Michaelis constants (K_M) and maximal velocities (V_{max}) were calculated as shown previously (13).

Kinetic Model of Airway ATP/Ado Regulation—This section outlines the theory and methodology used to build the mathematical model of airway nucleotide regulation on the apical surface of human airway epithelia. A biochemical network was derived using quantitative data gathered from the literature on nucleotide release (12, 20) and metabolism (13–15, 24, 26) by HBE cultures (Fig. 1). Because UTP levels are about 15% that of ATP (25) in the ASL layer, the influence of uridine nucleotides on ATP regulation was considered negligible. Therefore, the reactions governing ATP dephosphorylation to Ado and Ado deamination are as shown in Reactions 1–5,

$$ATP \rightarrow ADP + P_i$$
REACTION 1

$$ADP \rightarrow AMP + P_i$$
REACTION 2

$$AMP \rightarrow Ado + P_i$$
REACTION 3

$$Ado \rightarrow Ino$$
REACTION 4

$$ATP \rightarrow AMP + PP_i$$
REACTION 5

Each of the above reactions was assumed to follow Michaelis-Menten kinetics of the form shown in Equation 1,

$$\text{reaction rate} = \frac{V_{\max}^{(j)}[\text{S}]}{K_M^{(j)} + [\text{S}]} \quad \text{(Eq. 1)}$$

where [S] is the substrate concentration, and $V_{\max}^{(j)}$ and $K_M^{(j)}$ are the maximum velocity and Michaelis constant. The superscript *j* is used to index the multiple enzymes involved in the pathway. In contrast, the reversible ecto-AK Reaction 6,

$$\text{ATP} + \text{AMP} \leftrightarrow 2\text{ADP}$$
REACTION 6

which involves two binding sites, has been shown to follow a Bi Bi mechanism (32) as shown in Equation 2,

$$\text{reaction rate} = \frac{V_{\max}^{(f)}}{1 + \frac{K_{\text{ATP}}^{(f)}K_{\text{AMP}}^{(f)}}{[\text{ATP}][\text{AMP}]} + \frac{K_{\text{ATP}}^{(f)}}{[\text{ATP}]} + \frac{K_{\text{AMP}}^{(f)}}{[\text{AMP}]}} - \frac{V_{\max}^{(b)}}{1 + \left(\frac{K_{\text{ADP}}^{(b)}}{[\text{ADP}]}\right)^2 + \frac{2K_{\text{ADP}}^{(b)}}{[\text{ADP}]}} \quad \text{(Eq. 2)}$$

This expression is a generalization of Michaelis-Menten kinetics that relies on the same underlying assumptions. The model also incorporates the feed-forward inhibition of AMP hydrolysis by ATP and ADP. Experimental evidence indicates that ATP and ADP competitively bind to enzymes that catalyze AMP dephosphorylation (13, 33). Equation 3 was used to model this effect,

$$\text{reaction rate} = \frac{V_{\max}^{(j)}[\text{AMP}]}{K_M^{(j)}\left(1 + \frac{[\text{ATP}]}{K_{\text{ATP}}^{(in)}} + \frac{[\text{ADP}]}{K_{\text{ADP}}^{(in)}}\right) + [\text{AMP}]} \quad \text{(Eq. 3)}$$

Although it is possible that the inhibition constants $K_{\text{ATP}}^{\text{in}}$ and $K_{\text{ADP}}^{\text{in}}$ may differ for ecto-5′-NT and NSAP, these values were assumed identical for simplicity. The remaining elements that were incorporated into the model are the rates of ATP release and Ado/Ino uptake. In accordance with experimental observations (12), the basal rate of ATP release (J_{ATP}) was considered constant. Because Ado and Ino are taken back into the cell through CNT3, and therefore compete for access to the transporter, this effect is modeled using the following rates for Ado and Ino uptake as shown in Equations 4 and 5,

$$j_{\text{Ado}} = -\frac{V_{\max}^{(n,1)}[\text{Ado}]}{K_M^{(n,1)} + [\text{Ado}] + \frac{K_M^{(n,1)}}{K_M^{(n,2)}}[\text{Ino}]} \quad \text{(Eq. 4)}$$

$$j_{\text{Ino}} = -\frac{V_{\max}^{(n,2)}[\text{Ino}]}{K_M^{(n,2)} + [\text{Ino}] + \frac{K_M^{(n,2)}}{K_M^{(n,1)}}[\text{Ado}]} \quad \text{(Eq. 5)}$$

which allows for the possibility of different $V_{\max}$ and K_M values for the two molecules.

One of the functions of nucleotide release is to stimulate liquid secretion, which in turn may affect ASL nucleotide concentrations. Under static conditions, the basal rate of release does not maintain ATP at sufficiently high levels to activate P2 receptors (12). However, Ado levels generated from ATP metabolism under static conditions stimulate liquid secretion into the ASL layer via the A_{2B} receptor-CFTR pathway (17). Therefore, the model equations were derived for the general condition of a time-dependent ASL volume. To illustrate how the ASL volume enters the model, consider a simple case in which ATP is released into the ASL at a constant rate of J_{ATP} molecules/s, and then hydrolyzed by enzyme *E*. The surface area is denoted by *A*, and $[\mathbf{E}]_T$ represents the surface density of *E*, expressed in mol·cm^{-2}. If *V* indicates ASL volume, the equation governing ATP concentration is shown in Equation 6,

$$\frac{\text{d}[\text{ATP}]}{\text{d}t} = \frac{J_{\text{ATP}}}{V} - \frac{\frac{K_{\text{cat}}A}{V}[E]_T[\text{ATP}]}{K_M + [\text{ATP}]} - \frac{[\text{ATP}]}{V}\frac{\text{d}V}{\text{d}t} \quad \text{(Eq. 6)}$$

where $(k_{\text{cat}}A)/(V)[E]_T$ corresponds to maximum velocity ($V_{\max}$) and the last term models changes in ATP concentration because of the changing ASL volume. The considerations discussed above led to the formulation of five equations to describe the regulation of adenine nucleotides in the ASL layer (Equations 7–11). All model simulations were performed in MatLab (Mathworks, Natick, MA) using the ordinary differential equation solver of 15 s.

$$\frac{\text{d}[\text{ATP}]}{\text{d}t} = \frac{J_{\text{ATP}}}{V} - \frac{V_{\max}^{(1)}[\text{ATP}]}{K_M^{(1)} + [\text{ATP}]} - \frac{V_{\max}^{(2)}[\text{ATP}]}{K_M^{(2)} + [\text{ATP}]} - \frac{V_{\max}^{(3)}[\text{ATP}]}{K_M^{(3)} + [\text{ATP}]} - \frac{V_{\max}^{(10)}[\text{ATP}]}{K_M^{(10)} + [\text{ATP}]} - \frac{V_{\max}^{(f)}}{1 + \frac{K_{\text{ATP}}^{(f)}K_{\text{AMP}}^{(f)}}{[\text{ATP}][\text{AMP}]} + \frac{K_{\text{ATP}}^{(f)}}{[\text{ATP}]} + \frac{K_{\text{AMP}}^{(f)}}{[\text{AMP}]}} + \frac{V_{\max}^{(b)}}{1 + \left(\frac{K_{\text{ADP}}^{(b)}}{[\text{ADP}]}\right)^2 + \frac{2K_{\text{ADP}}^{(b)}}{[\text{ADP}]}} - \frac{[\text{ATP}]}{V}\frac{\text{d}V}{\text{d}t} \quad \text{(Eq. 7)}$$

$$\frac{\text{d}[\text{ADP}]}{\text{d}t} = \frac{V_{\max}^{(1)}[\text{ATP}]}{K_M^{(1)} + [\text{ATP}]} + \frac{V_{\max}^{(2)}[\text{ATP}]}{K_M^{(2)} + [\text{ATP}]} + \frac{V_{\max}^{(3)}[\text{ATP}]}{K_M^{(3)} + [\text{ATP}]} - \frac{V_{\max}^{(4)}[\text{ADP}]}{K_M^{(4)} + [\text{ADP}]} - \frac{V_{\max}^{(5)}[\text{ADP}]}{K_M^{(5)} + [\text{ADP}]} + \frac{2V_{\max}^{(f)}}{1 + \frac{K_{\text{ATP}}^{(f)}K_{\text{AMP}}^{(f)}}{[\text{ATP}][\text{AMP}]} + \frac{K_{\text{ATP}}^{(f)}}{[\text{ATP}]} + \frac{K_{\text{AMP}}^{(f)}}{[\text{AMP}]}} - \frac{2V_{\max}^{(b)}}{1 + \frac{K_{\text{ADP}}^{(b)}}{[\text{ADP}]}} - \frac{[\text{ADP}]}{V}\frac{\text{d}V}{\text{d}t} \quad \text{(Eq. 8)}$$

$$\frac{d[AMP]}{dt} = \frac{V_{max}^{(4)}[ADP]}{K_M^{(4)} + [ADP]} + \frac{V_{max}^{(5)}[ADP]}{K_M^{(5)} + [ADP]} + \frac{V_{max}^{(10)}[ATP]}{K_M^{(10)} + [ATP]} - \frac{V_{max}^{(f)}}{1 + \frac{K_{ATP}^{(f)}K_{AMP}^{(f)}}{[ATP][AMP]} + \frac{K_{ATP}^{(f)}}{[ATP]} + \frac{K_{AMP}^{(f)}}{[AMP]}}$$
$$+ \frac{V_{max}^{(b)}}{1 + \frac{K_{ADP}^{(b)}}{[ADP]}} - \frac{V_{max}^{(6)}[AMP]}{K_M^{(6)}\left(1 + \frac{[ATP]}{K_{ATP}^{(in)}} + \frac{[ADP]}{K_{ADP}^{(in)}}\right) + [AMP]} - \frac{V_{max}^{(7)}[AMP]}{K_M^{(7)}\left(1 + \frac{[ATP]}{K_{ATP}^{(in)}} + \frac{[ADP]}{K_{ADP}^{(in)}}\right) + [AMP]}$$
$$- \frac{V_{max}^{(8)}[AMP]}{K_M^{(8)}\left(1 + \frac{[ATP]}{K_{ATP}^{(in)}} + \frac{[ADP]}{K_{ADP}^{(in)}}\right) + [AMP]} - \frac{[AMP]}{V}\frac{dV}{dt} \quad \text{(Eq. 9)}$$

$$\frac{d[Ado]}{dt} = -\frac{V_{max}^{(9)}[Ado]}{K_M^{(9)} + [Ado]} - \frac{V_{max}^{(u,1)}[Ado]}{K_M^{(u,1)} + [ADO] + \frac{K_M^{(u,1)}}{K_M^{(u,2)}}[Ino]} + \frac{V_{max}^{(6)}[AMP]}{K_M^{(6)}\left(1 + \frac{[ATP]}{K_{ATP}^{(in)}} + \frac{[ADP]}{K_{ADP}^{(in)}}\right) + [AMP]}$$
$$+ \frac{V_{max}^{(7)}[AMP]}{K_M^{(7)}\left(1 + \frac{[ATP]}{K_{ATP}^{(in)}} + \frac{[ADP]}{K_{ADP}^{(in)}}\right) + [AMP]} + \frac{V_{max}^{(8)}[AMP]}{K_M^{(8)}\left(1 + \frac{[ATP]}{K_{ATP}^{(in)}} + \frac{[ADP]}{K_{ADP}^{(in)}}\right) + [AMP]} - \frac{[Ado]}{V}\frac{dV}{dt} \quad \text{(Eq. 10)}$$

$$\frac{d[Ino]}{dt} = \frac{V_{max}^{(9)}[Ado]}{K_M^{(9)} + [Ado]} - \frac{V_{max}^{(u,2)}[Ino]}{K_M^{(u,2)} + [Ino] + \frac{K_M^{(u,2)}}{K_M^{(u,1)}}[Ado]} - \frac{[Ino]}{V}\frac{dV}{dt} \quad \text{(Eq. 11)}$$

Linear Model for the Steady-state Nucleotide Concentrations—The biochemical data showed that, under physiological conditions, steady-state nucleotide concentrations are orders of magnitude lower than the K_M values of the enzymatic reactions (12). Hence, to a good approximation, the Michaelis-Menten reaction rates can be simplified (linearized) as shown in Equation 12,

$$\sum_{j=1}^{k} \frac{V_{max}^{(j)}[S]}{K_M^{(j)} + [S]} \sim \left(\sum_{j=1}^{k} \frac{V_{max}^{(j)}}{K_M^{(j)}}\right)[S] = P^{(k)} \cdot [S] \quad \text{(Eq. 12)}$$

where the parameter $P^{(k)}$ denotes the sum of the ratios of $V_{max}^{(j)}$ to $K_M^{(j)}$ for all enzymes catalyzing the same reaction. The expressions for Ado and Ino uptake can be simplified in a similar way. The reversible ecto-AK reaction (Reaction 6) is a second order reaction requiring two substrates and therefore does not contribute significantly to the regulation of ASL nucleotide concentrations under steady-state conditions. Also, steady-state ATP and ADP levels are 1000-fold lower than their K_i values for the feed-forward inhibition reaction (13) and therefore insufficient to inhibit AMP. Therefore, these equations were excluded from the linear model. Using these simplifications, Equations 7–11 can be approximated under steady-state conditions by the following set of linear Equations 13–17,

$$J_{ATP} - (P^{(1)} + P^{(5)})[ATP]_{ss} = 0 \quad \text{(Eq. 13)}$$

$$P^{(1)}[ATP]_{ss} - P^{(2)}[ADP]_{ss} = 0 \quad \text{(Eq. 14)}$$

$$P^{(5)}[ATP]_{ss} + P^{(2)}[ADP]_{ss} - P^{(3)}[AMP]_{ss} = 0 \quad \text{(Eq. 15)}$$

$$P^{(3)}[AMP]_{ss} - P^{(4)}[Ado]_{ss} - U^{(1)}[Ado] = 0 \quad \text{(Eq. 16)}$$

$$P^{(4)}[Ado]_{ss} - U^{(2)}[Ino]_{ss} = 0 \quad \text{(Eq. 17)}$$

where $U^{(1)}$ and $U^{(2)}$ result from linearizing the expressions for Ado (Equation 4) and Ino (Equation 5) uptake, respectively.

Statistical Analysis—All biochemical assays were conducted on HBE cultures from ≥5 subjects (±S.E.), and the mean experimental value was considered nonsignificantly different from the corresponding simulated value when <15% different.

RESULTS

Generation of the Experimental Data Set for Model Parameter Optimization—The strength of this model resides in the fact that all biochemical data were acquired from a single experimental system, polarized primary cultures of HBE cells maintained under air-liquid interface conditions and assayed in a physiological buffered solution (pH 7.5). Such consistency allowed us to combine data gathered over a decade into one experimental data set (Table 1, column A).

The first kinetic parameters of ATP and ADP hydrolysis measured on HBE cultures represent the sum of all apical ecto-ATPase and ecto-ADPase activities (26). More recently, we determined the kinetic properties of ecto-AK ($V_{max}^{(f)}$, $K_{ATP}^{(f)}$, $K_{AMP}^{(f)}$, $V_{max}^{(b)}$, and $K_{ADP}^{(b)}$; Table 1, column A) (28) and E-NPPs ($V_{max}^{(10)}$ and $K_M^{(10)}$; Table 1, column A) (24) on these cells. Based on this information, the kinetic measurements of ATP and ADP hydrolysis were repeated in the presence of the ecto-AK inhibitor, Ap_5A (28), to eliminate the influence of the nonlinear reaction (ATP + AMP ↔ 2ADP). Under these conditions, the ecto-ATPase and ecto-ADPase activities described by $V_{max}^{(1-5)}$ (Table 1, column A) combined the activities of two enzyme families: E-NTPDases and alkaline phosphatases. We also recently

TABLE 1

Kinetic parameters of ASL nucleotide/nucleoside release, uptake, and metabolism measured on primary cultures of HBE cultures or estimated by the model equations without/with ADP and AMP release

Unknown experimental values are labeled Unk. The units for V_{max} or J/V are nmol · min^{-1} · ml^{-1}, and the units for K_M are μM.

Reactions	Enzyme Identity	Parameters	[A] Experimental Data	REF[1]	[B] Simulation (J_{ATP})	[C] Simulation (J_{ATP},J_{ADP},J_{AMP})
	NTPDase 1/highNSAP	$V_{max}^{(1)}, K_M^{(1)}$	2.1, 12	26	9.7, 11.5	6.3, 16.3
ATP → ADP + Pi	NTPDase 3	$V_{max}^{(2)}, K_M^{(2)}$	8.1, 136	26	9.9, 186.1	15.5, 114.9
	lowNSAP	$V_{max}^{(3)}$ $K_M^{(3)}$	14.1, 451	26	22.1, 451.9	20.0, 418.0
ADP → AMP + Pi	NTPDase 1/highNSAP	$V_{max}^{(4)}, K_M^{(4)}$	1.4, 5	26	1.7, 5.3	0.5, 2.8
	NTPDase3/lowNSAP	$V_{max}^{(5)}, K_M^{(5)}$	9.1, 103	26	9.6, 151.5	10.7, 83.9
AMP → ADO + Pi	Ecto 5'-NT	$V_{max}^{(6)}, K_M^{(6)}$	1.8, 14	13	1.6, 12.4	1.7, 13.0
	highNSAP	$V_{max}^{(7)}, K_M^{(7)}$	4.2, 36	13	5.2, 36.3	6.2, 27.2
	lowNSAP	$V_{max}^{(8)}, K_M^{(8)}$	9.8, 717	13	8.0, 437.8	11.9, 694.9
ADO → INO	ADA1	$V_{max}^{(9)}, K_M^{(9)}$	0.6, 25	29	0.3, 28.2	0.3, 17.0
ATP → AMP + PPi	E-NPPs	$V_{max}^{(10)}, K_M^{(10)}$	0.9, 22	24	2.1, 7.5	1.2, 28.3
ATP + AMP → 2ADP	Ecto-AK (forward)	$V_{max}^{(f)}, K_{ATP}^{(f)}, K_{AMP}^{(f)}$	3.8, 23, Unk	28	1.7, 24.6, 13.5	2.2, 30.4, 24.7
ATP + AMP ← 2ADP	Ecto-AK (reverse)	$V_{max}^{(b)}$, $K_{ADP}^{(b)}$	1.8, 43	28	2.3, 72.3	2.2, 61.8
ATP release		$(J/V)_{ATP}$	0.0012	12	0.200	0.0011
ADP release		$(J/V)_{ADP}$	Unk			0.0131
AMP release		$(J/V)_{AMP}$	Unk			0.0125
ADO uptake	CNT3	$V_{max}^{(u,1)}, K_M^{(u,1)}$	0.12, 2.2	29	0.2, 1.2	0.2, 1.2
INO uptake	CNT3	$V_{max}^{(u,2)}, K_M^{(u,2)}$	Unk		0.2, 0.4	0.2, 1.2
Ki for ATP	Feed forward inhibition	$K_{ATP}^{(in)}$	7	13	66.7	28.4
Ki for ADP	Feed forward inhibition	$K_{ADP}^{(in)}$	10	13	41.8	20.4

[1] REF indicates references for the experimental data from our previous studies.

showed that HBE cells express NTPDase 1 and NTPDase 3 (15). It is important to note that the K_M corresponds to the substrate affinity of an enzyme, which is independent of cell type or expression level, whereas V_{max} constitutes a quantitative measure of the expression level of an enzyme (33). Because specific inhibitors of NTPDase 1 are currently unavailable, NTPDase 1 and NTPDase 3 were assigned to the parameter sets with K_M values approximating (±10%) their K_M (Table 1, column A), as reported for purified human NTPDase 1 (ATP, 10 μM; ADP, 20 μM) (34) and NTPDase 3 (ATP, 98 μM; ADP, 128 μM) (35).

We recently demonstrated that NSAP is the alkaline phosphatase isoform functionally expressed by human airway epithelia (13). Clinical assays, generally performed in basic solutions (pH 9–10), depict NSAP as a low affinity enzyme (K_M >400 μM) (23). However, NSAP has been shown to exhibit both low (lowNSAP; K_M >400 μM) and high (highNSAP; K_M =

TABLE 2

Kinetic parameters of ATP and ADP dephosphorylation by NSAP on primary cultures of HBE cells

Michaelis constants (K_M; μM) and maximal velocities (V_{max}: nmol · min^{-1} · ml^{-1}) were calculated from Woolf-Augustinson Hoftsee plots.

Reactions	Enzyme identity	Parameters	Experimental data
ATP → ADP + P_i	HighNSAP	V_{max}, K_M	1.0, 17
	LowNSAP	V_{max}, K_M	14.1, 451
ADP → AMP + P_i	HighNSAP	V_{max}, K_M	0.5, 11
	LowNSAP	V_{max}, K_M	5.9, 117

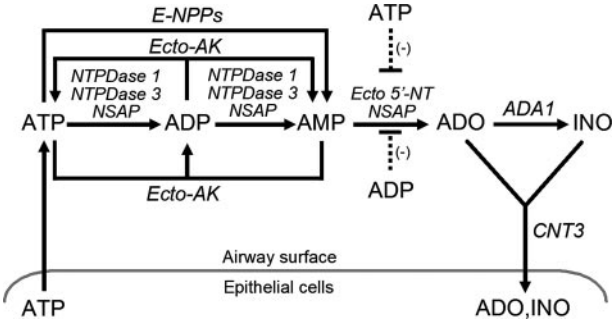

FIGURE 1. **Diagram of adenine nucleotides transport and metabolism on human bronchial epithelia.** Released by the epithelium, ATP is sequentially dephosphorylated into Ado by E-NPPs, ecto-AK, NTPDase 1, NTPDase 3, NSAP, and ecto-5′-NT. Ado is converted into Ino by ADA1, both returning to the cytosol via CNT3. The model also includes the feed-forward inhibition of Ado production by ATP and ADP.

12–20 μM) affinities for adenine nucleotides at pH 7.5 (36–38). We reported that airway NSAP hydrolyzes AMP with K_M values of 36 μM (highNSAP, $K_M^{(7)}$; Table 1, column A) and 717 μM (lowNSAP, $K_M^{(8)}K_M$; Table 1, column A) at pH 7.5 (13). Because the kinetic parameters of airway NSAP for ATP and ADP were unavailable, we conducted these experiments, as described previously (13) but in the presence of the ecto-AK inhibitor, Ap_5A (28). Two kinetic parameter sets were identified for ATP and ADP hydrolysis (Table 2), with K_M values within the ranges reported for lowNSAP and highNSAP activities (36–38). These values also approximated the K_M values of the high affinity and low affinity ecto-ATPase ($K_M^{(1)}$ and $K_M^{(3)}$) and ecto-ADPase ($K_M^{(4)}$ and $K_M^{(5)}$) activities (Table 1, column A). Because NSAP, NTPDase 1, and NTPDase 3 all support the dephosphorylation of ATP and ADP, enzyme activities with similar K_M values were combined and designated as the high affinity (NTPDase 1/highNSAP) and the low affinity (NTPDase 3/lowNSAP) enzymes (Table 1, column A).

The list of experimental data were completed by adding the kinetic parameters of ADA1 (29), the cellular uptake of Ado by CNT3 (29), the basal rate of ATP release (12), and the feed-forward inhibition of Ado production by ATP and ADP (13). Altogether, these assays and studies provided the experimental data set that was used to develop the mathematical model of nucleotide regulation on human airway epithelia (Table 1, column A).

Model Validation with Experimental Data—The model was tested by comparing simulated and previously reported experimental measurements of transient (26) and steady-state (12) nucleotide and nucleoside concentrations on the apical surface of HBE cells. We started our investigations using the multicomponent model (Fig. 1) described by Equations 7–11. Experimental values were available for all parameters from earlier

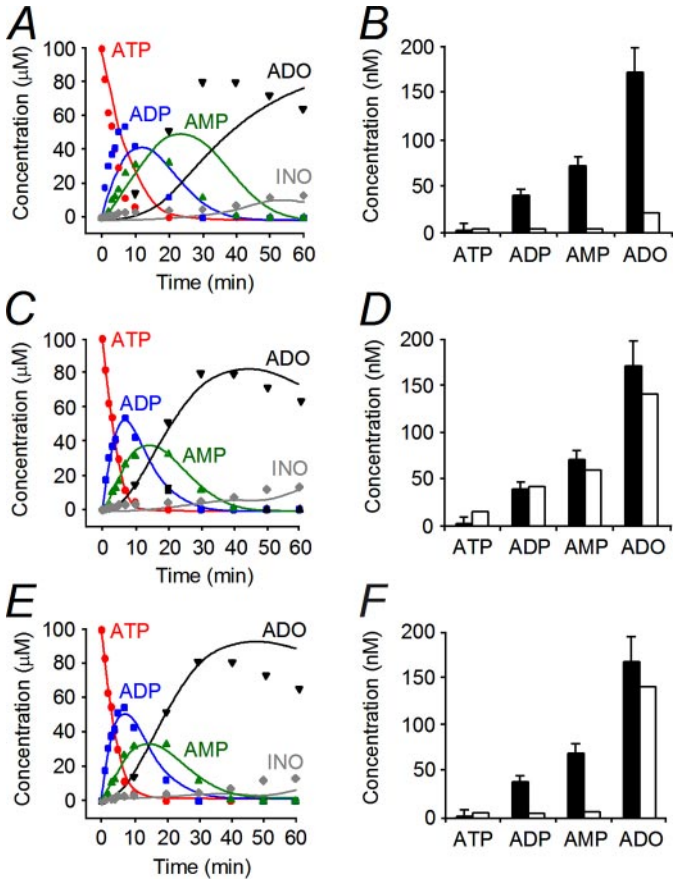

FIGURE 2. **Validation of the transient and steady-state concentration profiles generated by the nonlinear model without data fitting (*A* and *B*) or by data fitting using the MatLab nonlinear least square program without (*C* and *D*) or with (*E* and *F*) J_{ATP} fixed at the experimental value.** *A, C,* and *E,* simulation (*lines*) and experimental data (*symbols*; $n = 5$; S.E. <10% of mean) for nucleotide/nucleoside concentrations measured by HPLC of buffer samples collected from HBE cultures after the addition of 100 μM ATP ($n = 6$). *B, D,* and *F,* steady-state concentrations obtained by model simulation (*empty bars*) and experimental data (*filled bars*) from previous publications by our group ($n = 5$; ±S.E.) (12, 26).

studies (Table 1), except the K_M of ecto-AK for AMP and the K_M and V_{max} values of CNT3 for Ino. When used as free parameters to fit the data, considerable discrepancies were found between the simulated and experimental transient profiles of ATP hydrolysis (Fig. 2*A*) and steady-state concentrations (Fig. 2*B*). The performance of the model was considerably improved by using the experimental data set as initial guesses in the nonlinear least square fitting routine in MatLab (Mathworks, Natick, MA). Using this approach, the model closely reproduced the transient and steady-state profiles (Fig. 2, *C* and *D*). Among the 30 estimated parameters, only 6 were >2-fold different from the experimental values (Table 1, column B) as follows: high affinity ecto-ATPase ($V_{max}^{(1)}$), E-NPPs ($V_{max}^{(10)}$ and $K_M^{(10)}$), ecto-AK ($V_{max}^{(f)}$) and the feed-forward inhibition constants ($K_{ATP}^{(in)}$ and $K_{ADP}^{(in)}$). However, a 12-fold discrepancy persisted between measured and predicted ATP release rates. Similar experimental values were reported by different research groups using various techniques (10, 12, 20), ruling out experimental error as the source of discrepancy. On the other hand, if the rate of ATP release was held fixed at the experimental value and the other parameters free to be determined by data fitting,

TABLE 3
Steady-state concentrations (nM) calculated from the linear model without or with parameters of ADP and AMP release
Unk indicates unknown.

	ATP	ADP	AMP	Ado	Ino
Experimental data	2.2	38.7	70.2	168	Unk
Model optimization (J_{ATP})	3.9	2.8	4.6	15.3	6.7
Model optimization (J_{ATP}, J_{ADP}, J_{AMP})	4.0	38.1	70.3	231.7	102.0

the model reproduced the transient behavior of the system (Fig. 2*E*) but not the steady-state profile (Fig. 2*F*).

Steady-state Analysis with a Linear Model—In an attempt to resolve the differences between experimental and predicted steady-state ATP concentrations, we developed a linear model to describe the system near steady state, as described by Equations 13–17. The model was analyzed using two strategies. First, the experimental steady-state concentrations were used as inputs, and the model was solved for the parameter values. Because the steady-state Ino level cannot be measured by fluorescent HPLC, it was considered an unknown value in this procedure. In this case, solving the linear equations generated a negative Ino concentration, which is biologically impossible. Second, the experimental data set (Table 1, column A) was used as input parameters, and the model was solved for the steady-state concentration profile. This approach generated a good approximation of the experimental ATP concentration, but it resulted in estimated ADP, AMP, and Ado levels >10-fold lower than the experimental values (Table 3). Altogether, these results suggested that the model was incompatible with the experimental data and was therefore missing key components.

Our current knowledge on nucleotide release is limited to ATP because the inhibitor mixture designed to prevent nucleotide metabolism (20) interferes with fluorescence HPLC. However, emerging studies suggest that exocytosis mediates the release of ATP, ADP, and AMP from mammalian cells (39–41), including polarized epithelia (4, 7, 42). We recently demonstrated that human airway epithelia co-release ATP and mucin by Ca^{2+}-regulated exocytosis (42). During their maturation, secretory vesicles accumulate ATP- and UDP-sugars in concentrations ≥50-fold above cytosolic levels, a fraction of which is converted to ADP and UDP, and eventually to AMP and UMP (40). As a result, vesicle fusion to the apical membrane is expected to release ATP, ADP, and AMP into the ASL layer. These observations motivated the addition of terms describing ADP and AMP release to the mathematical model. Constant fluxes for ADP (J_{ADP}) and AMP (J_{ADP}) were added to the linear equations (Equations 13–17), and the values were adjusted so the model would generate steady-state concentrations closest to the experimental values. Table 3 shows that adding ADP and AMP release to the model eliminated the discrepancies between the experimental and predicted steady-state concentration profiles.

Reanalysis of the Nonlinear Model—The multienzyme model with the nonlinear equations (Equations 7–11) was updated to include terms describing the release of ADP (J_{ADP}/V in Equation 8) and AMP (J_{ATP}/V in Equation 9). The model was then refitted using the experimental data set (Table 1, column A) and the parameters of J_{ADP} and J_{AMP} (Table 1, column C). Under these conditions, the simulations closely reproduced the experimental transient (Fig. 3*A*) and steady-state (Fig. 3*B*) concentration profiles, and eliminated the 12-fold difference between measured and estimated J_{ATP}. Finally, the predicted V_{max} and K_M values (Table 1, column C) were in closest agreement with the experimental data (Table 1, column A). Collectively, these simulations and experiments suggest that the model captures all major elements of nucleotide regulation on human airway epithelia.

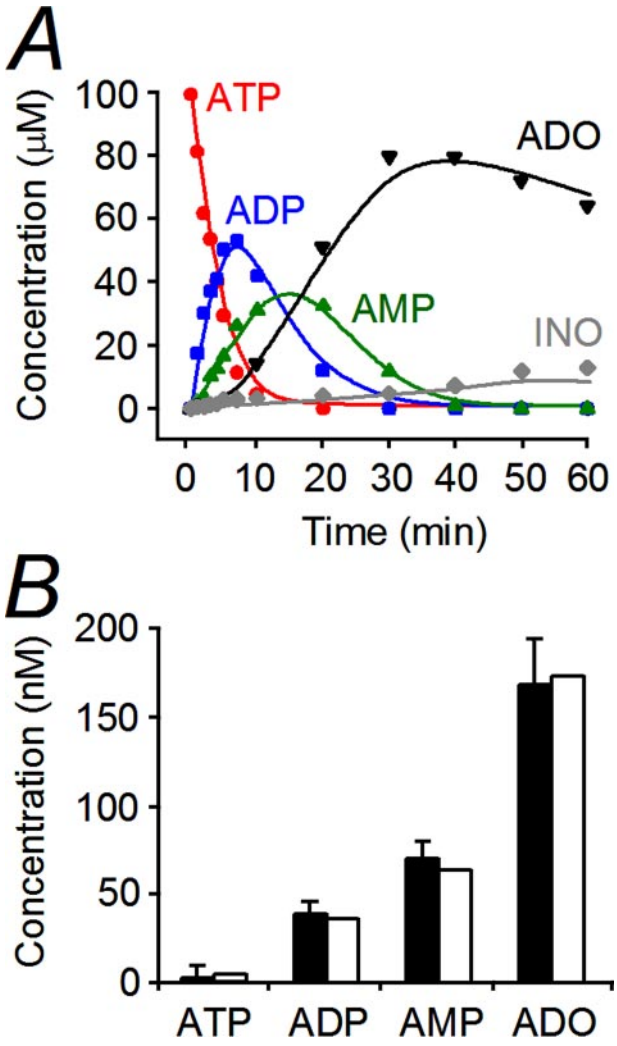

FIGURE 3. **Validation of the transient and steady-state concentration profiles generated by the model equations, including basal rates of ADP and AMP release.** *A,* simulated (*lines*) and experimental (*symbols*; $n = 5$; S.E. <10% of mean) transient nucleotide/nucleoside concentration profiles generated by the addition of 100 μM ATP on HBE cultures. *B,* simulated (*empty bars*) and experimental (*filled bars*) steady-state concentration profiles from previous publications by our group ($n = 5$; ±S.E.) (12, 26).

Impact of ASL Volume on Nucleotide Regulation—The model identified an important property of airway nucleotide regulation regarding ASL volume, which has been identified as a key determinant of mucus clearance (1, 2). Because the rate at which ATP release raises ATP concentration (J_{ATP}) and the maximum reaction velocity ($V_{max} = (k_{cat}A)/(V)[E]_T$), both scale inversely with ASL volume in Equation 6, the model predicts that steady-state concentrations are independent of ASL volume. Following a simulated 2-fold increase in ASL volume, which acutely dilutes ATP and ADP, nucleotide concentrations

are predicted to rapidly return to steady-state values (Fig. 4*A*). These simulation data were validated experimentally on HBE cultures using two luminometry assays, soluble luciferase and *S. aureus* protein A-luciferase attached to the epithelial surface. Fig. 4*B* shows that steady-state ATP and ADP levels, measured 60 min after the addition of 10–500 μl of phosphate-buffered saline, were unaffected by ASL volume changes. This result provides new insights into the biochemical processes supporting MCC. For instance, the airways of CF patients exhibit an ~70% reduction in ASL volume, which plays a critical role in airway obstruction (1, 2). Under steady-state conditions, the model predicts that ASL dehydration in CF does not concentrate, *i.e.* increase the availability of ATP and Ado for P2 and P1 receptor-mediated mucus clearance as a compensatory mechanism to restore ASL volume.

Model Adaptation to Mechanical Stress—Normal tidal breathing applies compressive and shear stresses on the airway walls that stimulate epithelial ATP release and ATP-mediated MCC (8, 10). This physiological response is particularly relevant to airway homeostasis as CCS mimicking tidal breathing was shown to restore ASL volume and mucus transport on the dehydrated airways of CF patients (10). Because the mathematical model was developed using experimental data acquired on static cultures, we tested its capacity to predict the ASL nucleotide and nucleoside concentrations maintained by mechanical stress mimicking tidal breathing. We recently demonstrated that CCS increases the rate of ATP release by 9.3-fold on HBE cultures (10). In this study, we conducted experiments to test the impact of CCS on the entire steady-state nucleotide concentration profile. Fig. 4*C* shows that CCS raised ATP, ADP, AMP, and Ado concentrations by 4–8-fold within the ASL layer. Model simulations were conducted to determine whether this response to mechanical stress was best fitted by an increase in the rate of ATP release or by concomitant increases in the release of several nucleotides. The equations solved with a 9.3-fold higher rate of ATP release (J_{ATP}; Table 1, column C) reproduced the effect of CCS on ATP but not on ADP or AMP (Fig. 4*C*). This simulation suggested that ATP release and metabolism were unable to account for the impact of CCS on ADP and AMP levels. Simultaneous 9.3-fold increases in J_{ATP} and J_{ADP} generated ATP and ADP levels within experimental range, whereas AMP levels remained >2-fold lower. The impact of CCS on the ASL concentration profile was best fitted by a model simulation in which J_{ATP}, J_{ADP}, and J_{AMP} were all 9.3-fold higher than base line. Altogether, these data are consistent with the general proposal that mechanical stress induces the release of all three nucleotides through exocytosis in polarized epithelia (39–42). Furthermore, they demonstrate the ability of the mathematical model to predict the complex behavior of ASL nucleotide regulation under static and dynamic conditions.

Novel Approach to Biochemical Network Analysis—Although several ectonucleotidases have been characterized on the apical surface of HBE cells (13–15, 24–29), the key enzyme(s) regulating nucleotide-mediated MCC remain unidentified because of the complexity of the multienzyme network. The mathematical model allowed us, for the first time, to determine the contribution of each enzyme and enzyme group to the regulation of both physiological and pathological ASL nucleotide concentra-

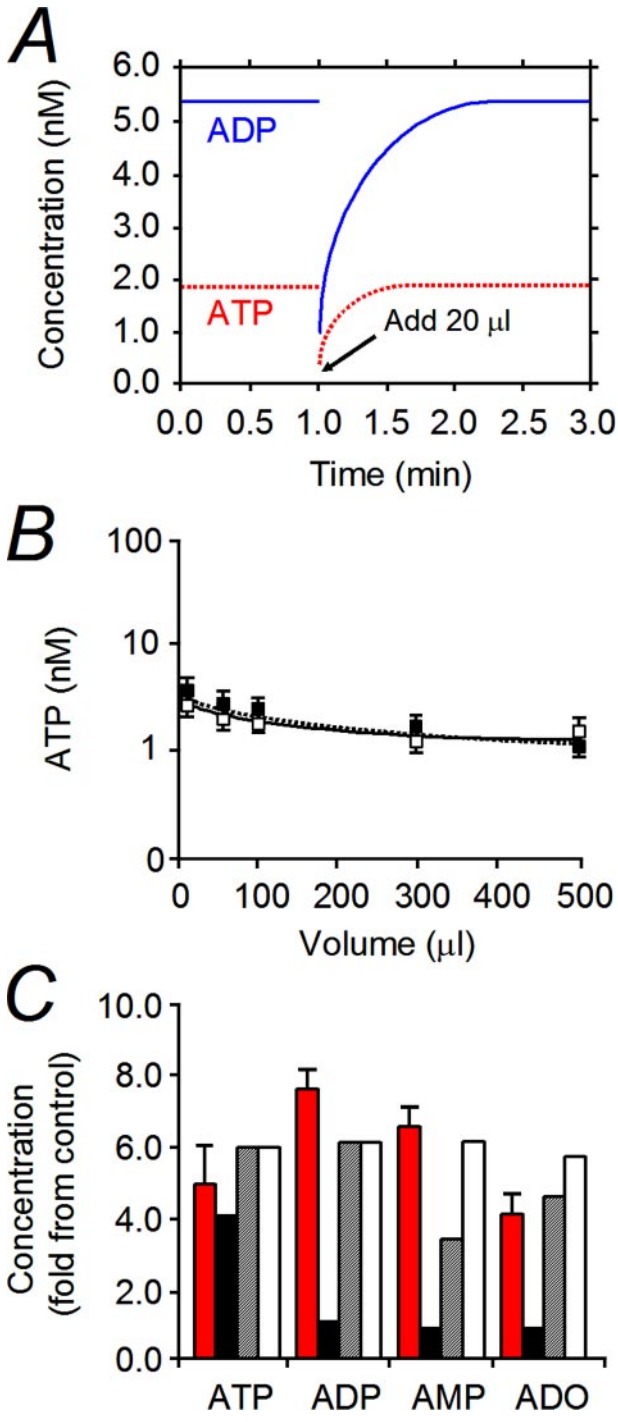

FIGURE 4. **Modeling the impact of ASL volume and mechanical stress mimicking tidal breathing on ASL nucleotide regulation.** *A,* model simulation of the impact of increasing ASL volume by 2-fold (20 μl) on steady-state ATP/ADP concentrations. *B,* model validation by biochemical measurements of steady-state ATP concentration using soluble luciferase (*solid black box*) or cell-attached *S. aureus* protein A-luciferase (*open box*) on HBE cultures after the addition of 1–500 μl of phosphate-buffered saline ($n = 5$; ±S.E.). *C,* impact of CCS (*solid red box*) on the steady-state concentration profile. HBE cultures were exposed 1 h to static conditions (control) or CCS mimicking tidal breathing (20 cm H_2O; 20 cycles/min) (10). Then ASL nucleotide concentrations were measured by HPLC ($n = 7$; ±S.E.). Model simulations conducted to reproduce the impact of CCS on the steady-state concentration profile by increasing the release rates of ATP (J_{ATP}; *black box*), ATP and ADP ($J_{ATP, ADP}$; *striped box*) or ATP, ADP and AMP ($J_{ATP, ADP, AMP}$; *open box*) by 9.3-fold (10). Values expressed as fold increase from static exposure.

tions. Several airway ectonucleotidases have been shown to hydrolyze ATP, ADP, and/or AMP as follows: NTPDase 1, NTPDase 3, NSAP, E-NPPs, and ecto-AK (14, 15, 28). Based on their kinetic properties, we hypothesized that specific enzymes regulate ASL nucleotide levels encountered under physiological conditions (<0.1 μM) (8, 12, 20), whereas others regulate higher ASL concentrations reached during tissue injury (0.1–1 μM) (43–46) or aerosolization (1–100 μM) for diagnostic (47, 48) or therapeutic (49–52) purposes. The biochemical network was first simplified by classifying the enzymes into the following two groups: 1) low affinity high capacity ($K_M \geq 50$ μM; NTPDase 3, lowNSAP), and 2) high affinity low capacity ($K_M < 50$ μM; NTPDase 1, E-NPPs, highNSAP, and ecto-AK). Model simulations were conducted by blocking the V_{max} of each enzyme (Table 1, column C) to reproduce the effects of selective inhibitors on HBE cultures. One of them, levamisole, inhibits both the high and low affinity activities of NSAP (13), which could introduce validation errors into group comparisons. This possibility was addressed by comparing the impact of eliminating highNSAP, lowNSAP, or high/low NSAP activities on ASL nucleotide regulation within the two concentration ranges of interest: aerosolized/pathological (10–100 μM) and physiological (0.1–1 μM). For V_{max} values corresponding to the total maximum activities of two enzymes, NTPDase 1/highNSAP ($V^{(1)}_{max}$ and $V^{(4)}_{max}$) and NTPDase 3/lowNSAP ($V^{(5)}_{max}$), NSAP activity was blocked by reducing the estimated parameter (Table 1, column C) proportionally by its experimental contribution (Table 2) to total enzyme activity (Table 1, column A). Fig. 5*A* shows that blocking highNSAP reduced the elimination rate of 100 μM ATP by <10%. In contrast, blocking lowNSAP or high/lowNSAP reproduced the effects of 10 mM levamisole on the HBE cultures and increased the half-life ($t_{1/2}$) of 100 μM ATP by 1.6-fold. Conversely, the metabolism of 1 μM ATP was not affected by blocking lowNSAP, whereas blocking highNSAP or high/lowNSAP mimicked the effects of levamisole with a 1.9-fold increase in the $t_{1/2}$ of ATP (Fig. 5*B*). These data indicate that lowNSAP and highNSAP activities exhibit negligible overlap, regulating excess and physiological ATP concentrations selectively. Consequently, model simulations in which both NSAP activities are blocked are expected to reproduce the effects of levamisole within the concentration range of interest.

We first acquired general information on the biochemical network by comparing the relative contribution of the low affinity and high affinity enzyme groups to the regulation of aerosolized/pathological nucleotide concentrations. Model simulations in which the kinetic parameters of the low affinity enzymes (high/lowNSAP and NTPDase 3) were blocked predicted a 4-fold decrease in elimination rate of 100 μM ATP and significant delays in the accumulation of ADP, AMP, and Ado (Fig. 5*C*). Comparable profiles were obtained experimentally using HBE cultures assayed with 100 μM ATP in the absence (control) or presence of an inhibitor mixture specific for the low affinity enzymes (Fig. 5*C*) as follows: 10 mM levamisole (NSAP) (13) + 10 μM NF-279 (NTPDase 3) (53). In contrast, model simulation in which all the high affinity enzymes (high/lowNSAP, NTPDase 1, E-NPPs, and ecto-AK) were blocked yielded minor modifications in the transient profile, with a 1.5-fold decrease in elimination rate of 100 μM ATP (Fig. 5*D*).

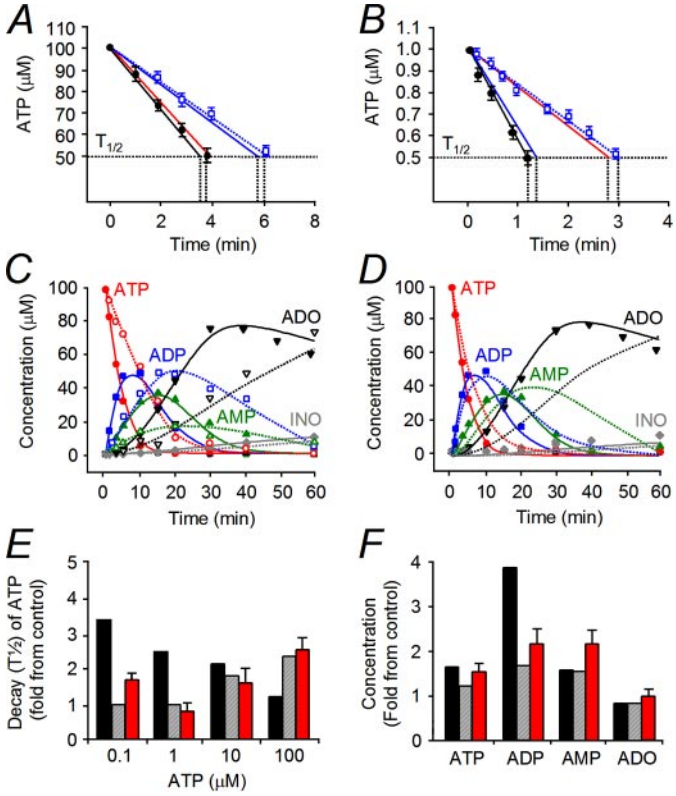

FIGURE 5. **Contribution of the low affinity and high affinity enzyme groups to ASL nucleotide regulation.** *A* and *B,* simulations comparing hydrolysis rates of 100 μM ATP (*A*) or 1 μM ATP (*B*) under control conditions (*solid black line*) or after blocking highNSAP (*solid red line*), lowNSAP (*solid blue line*), or both (high/lowNSAP) (*dashed blue line*). Validation conducted on HBE cultures for control conditions (●) and high/lowNSAP inhibition by 10 mM levamisole (*open blue box*). *C* and *D,* simulated metabolic profile for 100 μM ATP before (*solid line*) and after (*dashed line*) blocking the low affinity (*LA*; lowNSAP and NTPDase 3) (*C*) or high affinity (*HA*; NTPDase 1, highNSAP, E-NPPs, and ecto-AK) enzymes (*D*). Validation for the control (*C* and *D, filled symbols*) and low affinity block (*C*; *open symbols*) using an inhibitor mixture (10 mM levamisole + 10 μM NF-279) ($n = 5$; S.E. <10% of mean). *E,* simulated half-life ($t_{1/2}$) of 0.1–100 μM ATP generated by blocking the high affinity (*solid black box*) or low affinity (*striped box*) group, and experimental data (*solid red box*) for the low affinity block as above ($n = 5$; ±S.E.). *F,* simulated impact of blocking the high affinity (*solid black box*) or low affinity (*striped box*) group on the steady-state profile. Validation (*solid red box*) was by comparing ASL nucleotide levels before/after incubating HBE cultures with the low affinity inhibitor mixture ($n = 5$; ±S.E.).

Although experimental validation of the high affinity block awaits the identification of noncompetitive inhibitors for NTPDase 1 and E-NPPs, these data suggest that high ATP levels (>10 μM) are regulated mainly by the low affinity enzymes on airway epithelia.

Comparative analyses conducted over a broad range of ATP concentrations predicted a shift in the relative contribution of the high and low affinity enzyme groups. To carefully scrutinize the involvement of each group, the two NSAP activities were analyzed independently. Model simulations in which the high affinity enzymes (highNSAP, NTPDase 1, E-NPPs, and ecto-AK) or the low affinity enzymes (lowNSAP and NTPDase 3) were blocked raised the $t_{1/2}$ of 100 μM ATP by 1.2- and 2.3-fold, respectively (Fig. 5*E*). Although the $t_{1/2}$ of 10 μM ATP would be equally affected by either group, the high affinity group is predicted to dominate at lower ATP concentrations. These simulations were reproduced experimentally on HBE cultures with a

low affinity inhibitor mixture (10 mM levamisole + 10 μM NF-279) (Fig. 5*E*). The model suggests that the higher contribution of the low affinity group measured experimentally for 0.1 μM ATP reflects the inhibitory effect of levamisole on highNSAP. Together, simulated and experimental results support a major role for high affinity enzymes in the regulation of ASL ATP within the effective concentration range of $P2Y_2$ receptors (0.01–1 μM) (16, 17).

Recent studies showed that ASL nucleotide metabolism is accelerated in chronic lung diseases, including CF, chronic obstructive pulmonary disease, and primary ciliary dyskinesia (14), which could compromise nucleotide-mediated MCC (19, 52). Consequently, activation of $P2Y_2$ receptors by aerosolized nucleotides is being tested as a therapy for CF (52, 54). As an alternative strategy to raise steady-state ASL ATP concentration, we conducted simulations to test the potential of an aerosolized inhibitor mixture against specific enzymes. As expected from their kinetic properties, model simulations in which the low affinity enzymes (lowNSAP and NTPDase 3) were blocked predicted a <2-fold increase in steady-state nucleotide concentrations (Fig. 5*F*). This simulation was reproduced experimentally by assays conducted on HBE cultures exposed to the low affinity inhibitor mixture (10 mM levamisole + 10 μM NF-279) (Fig. 5*F*). Because levamisole does not discriminate between the lowNSAP and highNSAP activities, these assays demonstrate that NSAP does not contribute significantly to the regulation of steady-state ATP concentrations (*i.e.* <0.1 μM) on airway epithelial surfaces. To our surprise, the model predicts that the steady-state nucleotide levels are sensitive to the high affinity enzyme group with respect to ADP but not ATP (Fig. 5*F*), which suggested the influence of a nonlinear component within the biochemical network.

The properties of the reversible ecto-AK reaction suggest that the net directionality depends on the relative substrate concentrations (Fig. 6*A*). Micromolar ATP, encountered during injury or aerosolization, would drive the forward reaction, whereas steady-state conditions would favor the reverse reaction because of the relatively high ADP concentration (Table 3). Therefore, simulations and assays were designed to test whether ecto-AK influences the ATP/ADP concentration ratio on airway epithelial surfaces in these two situations (Fig. 6*A*). Model simulations predicted that blocking ecto-AK would not affect the metabolism of 100 μM ATP (Fig. 6*B*) or the steady-state concentration profile (Fig. 6*E*). These simulated data were reproduced experimentally for the transient (Fig. 6*B*) and steady-state (Fig. 6*E*) concentration profiles by HBE cultures exposed to the vehicle control or buffer containing the ecto-AK inhibitor, 0.5 mM Ap_5A (28). We next tested the hypothesis that ecto-AK activity may be significant within a functional unit addressing a specific nucleotide concentration range. Fig. 6*C* shows that blocking ecto-AK is not expected to influence the metabolic profile of 100 μM ATP regulated by the low affinity enzymes, *i.e.* determined in the absence of the other high affinity enzymes. In contrast, model simulations and experimental data suggest that ecto-AK contributes to the regulation of ASL nucleotides under conditions where the high affinity enzyme activities predominate. First, the model predicts that blocking ecto-AK would not affect the elimination rate of 100 μM ATP

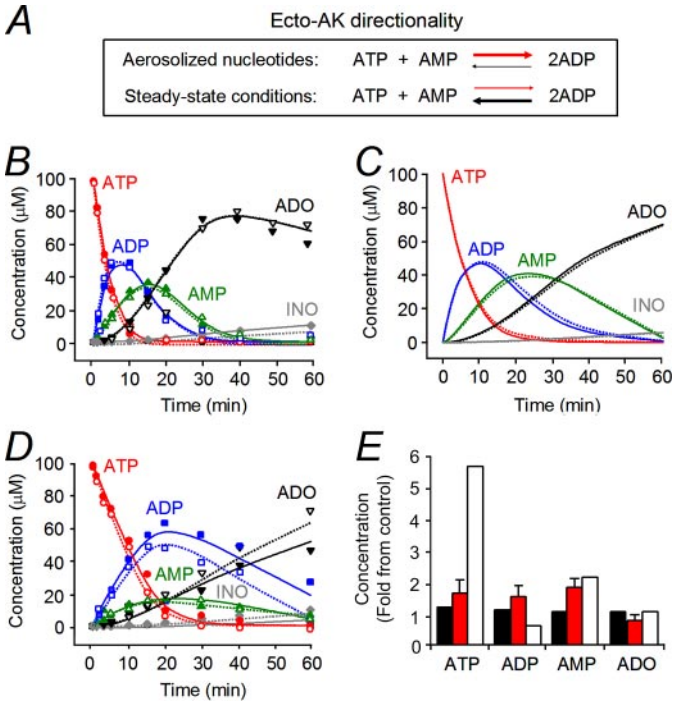

FIGURE 6. **Role of ecto-AK in ASL nucleotide regulation.** *A,* reaction directionality during nucleotide aerosolization (>10 μM ATP) and under steady-state conditions (1–10 nM ATP) with ADP/ATP >20 (Table 3). *B–D,* simulations (*lines*) of the impact of blocking ecto-AK on the metabolism of 100 μM ATP (*B*) in the presence of all enzymes and after blocking (*C*) the high affinity (NTPDase 1, highNSAP, and E-NPPs) or (*D*) low affinity (*LA*; lowNSAP and NTPDase 3) enzymes. *B,* validation using HBEs pretreated with the vehicle (*closed symbols*) or the ecto-AK inhibitor (0.5 mM Ap_5A; *open symbols*). *D,* validation on HBEs pretreated with the low affinity inhibitor mixture (10 mM levamisole + 10 μM NF-279) without (*closed symbols*) or with (*open symbols*) 0.5 mM Ap_5A ($n = 6$; S.E. < 10% of mean). *E,* impact of blocking ecto-AK on the steady-state profile by stimulation (*solid black box*) or exposing HBEs to 0.5 mM Ap_5A (*solid red box*) ($n = 5$; ±S.E.). Data were compared with the simulated impact of blocking the other high affinity enzymes (*open box*).

by a high affinity biochemical network, *i.e.* determined in the absence of the low affinity enzymes (Fig. 6*D*). However, when ADP concentration rises above that of ATP (~20 min), the absence of ecto-AK would be associated with higher rates of ADP elimination and Ado accumulation (Fig. 6*D*). Similar results were obtained experimentally with HBE cultures using the low affinity inhibitor mixture (10 mM levamisole and 10 μM NF-279) with/without 0.5 mM Ap_5A (Fig. 6*D*). These data were also consistent with the behavior of ecto-AK reported on HBE cultures exposed to an ATP concentration (1 μM) (28) predicted to be regulated predominantly by high affinity enzymes (Fig. 5*E*). The reverse ecto-AK reaction would compete with the high affinity ADP-hydrolyzing enzymes to trap adenine nucleotides into a trans-phosphorylation cycle (28). These findings suggest that airway ecto-AK regulates ASL nucleotide levels within a high affinity biochemical network exposed to a high ADP/ATP concentration ratio.

Based on this information, we revisited the impact of ecto-AK on ASL nucleotide regulation at steady-state conditions, which is expected to favor the reverse ecto-AK reaction (2ADP → ATP + AMP) (Fig. 6*A*) because of the high ADP/ATP ratio (~20; see Table 3). A model simulation with a high affinity inhibitor mixture, excluding the ecto-AK inhibitor, resulted in a 6-fold increase in steady-state ATP concentration (Fig. 6*E*),

compared with 2-fold for a complete high affinity block (Fig. 5*F*). The physiological relevance of this information is illustrated by the fact that a comparable increase in ASL ATP level was generated by CCS mimicking normal tidal breathing (Fig. 4*C*), which restored normal ASL height and mucus transport on the dehydrated airway epithelial surfaces of CF patients (10). The mathematical model of ASL nucleotide regulation therefore identified the key enzymes regulating ASL ATP and proposes a novel approach for the treatment of airway obstruction in CF, an aerosolized inhibitor mixture against high affinity NTPDase 1 and E-NPPs.

Adenosine Regulation in Airway Defenses—The model was instrumental to our investigation of airway Ado regulation, supplementing the biochemical assays with simulated information that would not be available experimentally. First, we modeled the relative contribution of the two ectonucleotidases supporting the conversion of AMP to Ado on airway epithelial surfaces, NSAP and ecto-5′-NT (13). Model simulations were run by blocking the parameters of the following: 1) ecto-5′-NT; 2) high/lowNSAP toward AMP [NSAP (AMP)], or 3) high/lowNSAP toward ATP, ADP, and AMP [NSAP (all)]. These simulations were verified by biochemical assays conducted on HBE cultures before and after the inhibition of ecto-5′-NT (10 mM concanavalin A) (13, 55) or NSAP (10 mM levamisole) (13, 56). Although blocking all parameters of NSAP would mimic the effects of levamisole, we tested whether the concomitant reductions in ecto-ATPase and ecto-ADPase activities would influence the feed-forward inhibition of Ado accumulation (Equation 3) (13). Hence, all simulations and assays were initiated with ATP to probe the response of the entire biochemical network.

Comparative analysis conducted over a range of ATP concentrations revealed a shift in the relative contribution of ecto-5′-NT and NSAP (Fig. 7, *A–C*). Both simulated and experimental data showed that ecto-5′-NT dominates at physiological ATP levels (0.1–1.0 μM), as indicated by larger reductions in the accumulation rate of Ado (Fig. 7, *A* and *B*). In contrast, Ado production from 10 μM ATP would be equally reduced by blocking ecto-5′-NT or NSAP (AMP) (Fig. 7*C*). Interestingly, an intermediate response was predicted by blocking NSAP (all) (Fig. 7*C*) or measured experimentally with levamisole (Fig. 7*C*). These data suggest that levamisole increases the availability of ATP and ADP for the feed-forward inhibition of Ado production by the remaining enzyme, ecto-5′-NT.

Model simulations were designed to evaluate the physiological relevance of feed-forward inhibition for airway homeostasis by calculating the time required for 1–1000 μM ATP to generate an Ado concentration equivalent to the EC_{50} of A_{2B} receptors (0.3 μM) (16, 17). Both simulated and biochemical data demonstrated that the delay to reach 0.3 μM Ado is influenced by the ASL ATP concentration in a biphasic manner (Fig. 7*D*). A relatively long delay would be expected for concentrations (*i.e.* 1 μM ATP) below the catalytic capacity of most airway ectonucleotidases (Table 1, column A). In the 10–100 μM ATP range, both enzymes efficiently converted AMP to Ado, whereas longer delays are required for ATP levels challenging their V_{max}.

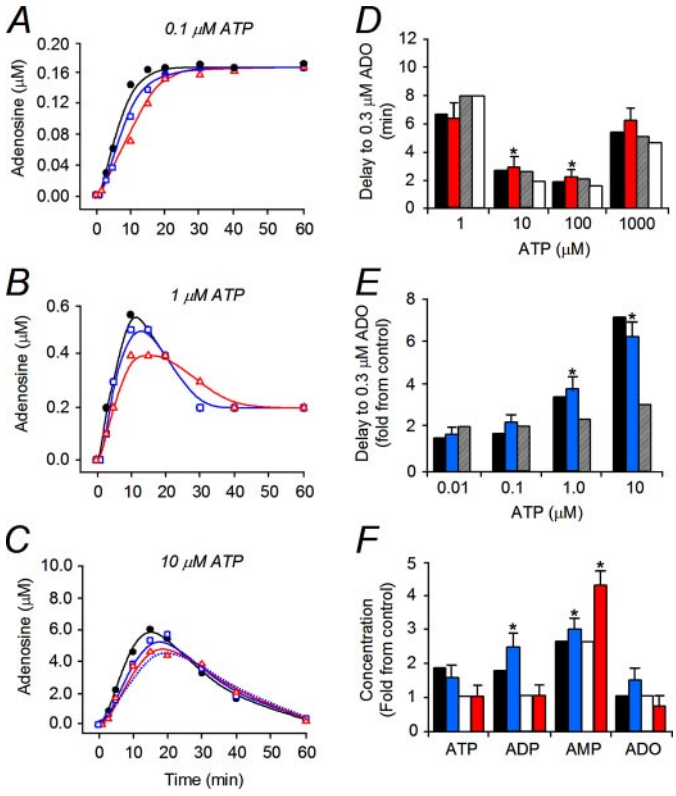

FIGURE 7. **Relative contribution of ecto-5′NT and NSAP to Ado regulation.** *A–C,* simulated (*lines*) and experimental (*symbols*) time courses of Ado accumulation from 0.1 to 10 μM ATP under control conditions and after blocking ecto-5′-NT (*solid red line*) or NSAP (*solid blue line*) activities. For NSAP, simulations were run by blocking the parameters regulating AMP (NSAP (AMP)) (*dashed blue line*) or all nucleotides (NSAP (all)) (*solid blue line*). Experimental data using HBE cultures were incubated with 0.1–10 μM ATP, without/with an inhibitor of ecto-5′-NT (10 mM concanavalin A) (*open red triangle*), or NSAP (all) (10 mM levamisole) (*open blue box*) ($n = 6$; S.E. $< 10\%$ of mean). *D,* simulated (*solid black box*) and experimental (*solid red box*) delay to the accumulation of 0.3 μM Ado from 1 to 1000 μM ATP. Simulations also compared the impact of blocking ecto-5′-NT with (*striped box*) or without (*open box*) feed-forward inhibition ($K^{(in)}_{ATP}$, $K^{(in)}_{ADP}$ block; Table 1, column C). *E,* simulated (*solid black box*) and experimental (*solid blue box*; $n = 5, p < 0.05$) impact of blocking NSAP (all) on the delay to reach 0.3 μM Ado (fold from controls in *D*). Simulated impact of blocking both NSAP (all) and feed-forward inhibition (*striped black box*) is shown. *F,* simulated impact of blocking NSAP (all) (*solid black box*) or ecto-5′-NT (*open box*) on the steady-state profile. Experimental block of NSAP (all) (*solid blue box*) or ecto-5′-NT (*solid red box*) was obtained by measuring nucleotide levels before/after incubating cultures with the inhibitors ($n = 5$, $p < 0.05$).

The mathematical model was able to identify the enzyme targeted by feed-forward inhibition using simulations that cannot be reproduced experimentally: by blocking the kinetic constants ($K^{(in)}_{ATP}$ and $K^{(in)}_{ADP}$; Table 1, column C). We compared the impact of blocking each AMP-hydrolyzing enzyme on the ATP-mediated regulation of Ado production in the presence or absence of feed-forward inhibition. Model simulations in which the V_{max} of ecto-5′-NT activity was blocked resulted in slightly longer Ado delays ($< 30\%$) at all ATP concentrations, which were partially reduced to control values by blocking the inhibition constants (Fig. 7*D*). These simulations predict a weak control of feed-forward inhibition over the remaining enzyme, NSAP, which may be ascribed to its capacity to eliminate ATP and ADP in close vicinity to the catalytic site.

The reciprocal simulation exposed a strong relationship between ASL ATP concentration and Ado production by ecto-

5′-NT. The time required for Ado to reach the EC_{50} of A_{2B} receptors (0.3 μM) (16, 17) increased by up to 6-fold when ecto-5′-NT dominated, *i.e.* in the absence of NSAP, with a regulatory threshold of 1 μM ATP (Fig. 7*E*). These simulations were reproduced by HBE cultures pretreated with the NSAP inhibitor (10 mM levamisole). The model predicts that this relationship would be completely abrogated by simultaneously blocking NSAP (all) and the feed-forward inhibition (Fig. 7*E*). The mathematical model therefore provided new insights into the biochemical processes regulating ASL Ado, which would not have been available otherwise. The simulations predict that feed-forward inhibition targets specifically Ado production by ecto-5′-NT on HBE surfaces. However, whereas the sensitivity of ecto-5′-NT activity to $\geq$1 μM ATP is consistent with the properties of the vascular model of nucleotide regulation (57–59), airway epithelia seldom experience such high ATP concentrations, except locally during injury or aerosolization.

Finally, we determined the contribution of NSAP and ecto-5′-NT to the regulation of the steady-state nucleotide concentrations. The model predicts that NSAP inhibition would raise ATP, ADP, and AMP concentrations by 1.4-, 2.5-, and 2.8-fold, respectively (Fig. 7*F*). This inverse relationship between NSAP activity and the degree of phosphorylation of the substrate was closely reproduced experimentally by levamisole on HBE cultures (Fig. 7*F*) and is consistent with the properties of the purified enzyme: ATP $<$ ADP $<$ AMP (60, 61). In contrast, model simulations in which ecto-5′-NT activity was eliminated only increased AMP concentration, in agreement with the substrate specificity of the enzyme (56). These results were reproduced by HBE cultures exposed to the selective inhibitor, concanavalin A (Fig. 7*F*). Altogether, these data demonstrate that the model captures the contributions of ecto-5′-NT and NSAP to the regulation of steady-state nucleotide concentrations. On the other hand, inhibiting ecto-5′-NT or NSAP did not influence the steady-state concentration of Ado, which suggests that one AMP-hydrolyzing enzyme may be sufficient under conditions where AMP concentration is $>$100-fold lower than their K_M values.

DISCUSSION

This study presents the first mathematical model of extracellular nucleotide and nucleoside regulation for the respiratory system. Based on experimental data reported in the literature (12, 13, 20, 26, 28, 29), and acquired in this study, for polarized HBE cultures, Equations 7–11 were designed to incorporate all known factors regulating ASL nucleotides and Ado as follows: epithelial ATP release, the reactions mediating the surface conversion of ATP into ADP, AMP, and Ado, the surface elimination of Ado by deamination and cellular uptake, the trans-phosphorylating ecto-AK activity, and the feed-forward inhibition of Ado production by ATP and ADP. The simulations closely reproduced the transient and steady-state concentration profiles generated on the apical surface following the addition of ATP. However, regardless of the fitting strategy, a 12-fold difference persisted between the simulated and experimental rates of ATP release, suggesting the model was missing key elements.

The current information on the mechanisms of nucleotide release is derived from measurements of ATP release (62, 63). Yet recent breakthroughs in our understanding of exocytosis support the notion that nucleotides, in addition to ATP, are also released via this route by a variety of cell types (4, 39–41), including HBE cells (42). During their maturation, the vesicles accumulate ATP, ADP, and AMP, which are released during exocytosis (39–41). Importantly, the addition of terms describing ADP and AMP release provided the best fit of the experimental data, as well as the transient and steady-state concentration profiles. Furthermore, it resolved the discrepancy between simulated and experimental rates of ATP release.

The resulting model was validated by testing the impact of mechanical stress on ASL nucleotide regulation. Airway epithelia, *in vivo*, are subjected to mechanical forces imparted by tidal breathing, which are known to stimulate ATP release (8, 10). We recently showed that CCS mimicking normal tidal breathing causes a 9.3-fold increase in the rate of ATP release from HBE cultures (10). In this study, we showed that CCS raises the ASL concentrations of ATP, ADP, AMP, and Ado by 4–7-fold. Model simulations in which J_{ATP} was increased 9.3-fold reproduced the effects of CCS on ATP but not on the other nucleotides. The model therefore predicted that mechanical stress-induced ATP release and surface metabolism are unable to account for the effects of CCS on the ASL nucleotide composition. In fact, the best fit was obtained by raising simultaneously J_{ATP}, J_{ADP}, and J_{AMP} by 9.3-fold. These results support the importance of including parameters for the release of all three nucleotides into the mathematical model of ASL nucleotide regulation. Furthermore, they illustrate the capacity of the model to predict the impact of physiological phenomena such as breathing on ASL nucleotide regulation.

Multiple ATP-hydrolyzing enzymes compete for the same pool of nucleotides within the ASL layer. The development of a mathematical model incorporating all the ectonucleotidases provided, for the first time, an invaluable tool to assess their individual contribution within the multienzyme system. The complex biochemical network was simplified by sorting the enzymes into kinetically distinct groups as follows: low affinity high capacity ($K_M > 50$ μM; lowNSAP and NTPDase 3) and high affinity low capacity ($K_M < 50$ μM; highNSAP, E-NTPDase 1, E-NPPs and ecto-AK) (26, 64). Model simulations accurately predicted the predominant role of the low affinity group in the regulation of high ATP concentrations ($>$1 μM) (43–46), as demonstrated on HBE cultures using selective inhibitors of NSAP (10 mM levamisole) (13) and NTPDase 3 (10 μM NF-279) (53). Therapies inhibiting these ectoenzymes could potentially accentuate airway epithelial apoptosis (65, 66) and inflammatory responses (45) because of increased ATP-mediated activation of $P2X_7$ receptors, which are up-regulated in lung diseases (67). In addition, these enzymes are likely responsible for the rapid elimination of aerosolized nucleotides (1–100 μM) used to diagnose asthma and chronic obstructive pulmonary disease (ATP and AMP) (47, 48), for the treatment of CF and primary ciliary dyskinesia (UTP) (49–52) and in animal studies (48, 68, 69).

The model predicts that high affinity enzymes play a major role in the regulation of ATP within the physiological concentration range encountered on airway epithelial surfaces (8, 12, 20). The recent report that CCS-mediated increase in ASL ATP

level restores ASL volume and mucus transport on dehydrated HBE cultures from CF patients (10) motivated the search for an inhibitor mixture against the high affinity enzymes to enhance $P2Y_2$ receptor-mediated mucus clearance. However, the model predicts that blocking all four enzymes would raise ADP concentrations, instead of ATP. An explanation was provided by separating the high affinity enzymes into linear and nonlinear components. Inhibition of the enzymes supporting the linear reactions (ATP → ADP → AMP; NTPDase 1, E-NPPs and highNSAP) is expected to raise the concentrations of all the released nucleotides. In contrast, the directionality of the reversible ecto-AK reaction (ATP + AMP ↔ 2ADP) would be influenced by the ASL nucleotide composition. Model simulations and biochemical assays suggest that ecto-AK does not influence the elimination of high ATP concentrations (>10 μM). However, blocking ecto-AK significantly modified the transient metabolic profile generated by the high affinity enzyme group once ADP level exceeded that of ATP by >3-fold, as depicted by enhanced ADP, but increased Ado, accumulation. This behavior is consistent with the substrate requirements of the reversible ecto-AK reaction. The forward reaction (ATP + AMP → 2ADP) is limited on airway epithelia by the high ATP/AMP ratio maintained through efficient conversion of AMP to Ado. In contrast, the reverse reaction (2ADP → ATP + AMP) is favored once ADP concentration exceeds that of [ATP + AMP]. However, the ATP generated by ecto-AK would be rapidly dephosphorylated by the high affinity ecto-ATPases (NTPDase 1, E-NPPs, and highNSAP). Consequently, these data suggest that removing the strong competitive effect of the linear high affinity enzymes may allow ecto-AK to raise ATP concentrations within a nucleotide mixture dominated by ADP.

Based on this analysis of the high affinity group, we evaluated the role of ecto-AK under steady-state conditions, in which ASL exhibits an ADP/ATP concentration ratio of ~20 (Table 3). The model predicts that a high affinity inhibitor mixture, excluding the ecto-AK inhibitor (Ap_5A), would raise the ASL ATP concentration by ~6-fold. The therapeutic potential of this approach is illustrated by the fact that CCS mimicking normal breathing produced a similar increase in ASL ATP level (Fig. 4*C*), which restored mucus transport on the airway epithelial surfaces of CF patients (10). The physiological importance of ecto-AK for the regulation of steady-state nucleotide levels was also demonstrated in human hepatocytes, where it regulates $P2Y_{13}$ (ADP) receptor-mediated high density lipoprotein endocytosis (70). The ecto-AK inhibitor stimulated high density lipoprotein endocytosis in the absence of exogenous substrates, supporting a significant role in cholesterol transport under steady-state conditions. Altogether, the model and experimental data suggest that aerosolization of an inhibitor mixture against the high affinity enzymes (excluding Ap_5A) may stimulate airway clearance in CF patients. The fact that blocking NSAP did not affect the steady-state ATP level suggests that levamisole may be omitted. Further refinement of the high affinity enzyme inhibitor mixture for the treatment of obstructive lung diseases awaits the discovery of specific noncompetitive inhibitors for NTPDase 1 and the E-NPPs.

The regulation of ASL nucleotides through cell surface metabolism leads to the accumulation of another important signaling molecule for airway defenses, *i.e.* Ado. We previously demonstrated that two ectoenzymes contribute to the production of Ado on airway epithelial surfaces, ecto-5′-NT and NSAP (13). Although their characterization was conducted using AMP as initial substrate (13), this study documented the impact of the entire biochemical network on ASL Ado production using ATP as initial substrate. Based on model simulations and biochemical assays, we identified a negative relationship between ATP ≥1 μM and the time required for Ado concentration to reach the EC_{50} of A_{2B} receptors for CFTR activation (0.03 μM) (16, 17). Model simulations, in which the kinetic constants $K_{ATP}^{(in)}$ and $K_{ADP}^{(in)}$ were blocked, suggest that this relationship is caused by feed-forward inhibition of ATP on ecto-5′-NT, but not on NSAP. These data are in agreement with the reported inhibition of purified ecto-5′-NT by ATP and ADP (71, 72). Although the inhibitory mechanism has not been identified, the insensitivity of NSAP may be partially because of its capacity to eliminate ATP and ADP. Altogether, these results emphasize the critical importance of studying the properties of ectonucleotidases using experimental designs accounting for the entire biochemical network, as the suppression of ecto-5′-NT activity by ATP would have been missed by protocols isolating the AMP → Ado reaction.

In human airways, feed-forward inhibition is not expected to play a significant role in the regulation of purinergic signaling, as epithelial surfaces are not normally exposed to >1 μM ATP (73–75). However, this regulatory mechanism may become relevant during injury-induced ATP release to prevent A_{2B} receptor desensitization (76) and/or excessive inflammatory responses caused by chronically high Ado concentrations (77). But even under these circumstances, NSAP activity would be expected to compensate for the reduction in ecto-5′-NT activity caused by excess ATP. Consequently, this regulatory mechanism may be more relevant for purinergic signaling in tissues expressing ecto-5′-NT, with little or no NSAP. For instance, feed-forward inhibition is not detected on vascular smooth muscle cells (78), which express NSAP (79). In contrast, endothelial surfaces do not express NSAP (80) and exhibit an inhibitory effect of ADP on ecto-5′-NT activity (59, 81). Because ADP activates platelets and Ado suppresses their activation (31, 82), feed-forward inhibition was proposed to regulate thrombus formation during endothelial repair. A mathematical model of extracellular nucleotide metabolism on endothelial cells predicts an inhibition of Ado production by 1–10 μM ADP (57–59). Because activated platelets release >1 mM ADP on endothelial surfaces (31), feed-forward inhibition would create a time gap between ADP- and Ado-mediated responses, allowing sufficient time to consolidate the thrombus while minimizing spread beyond the site of damage. Consequently, two factors determine the importance of feed-forward inhibition for purinergic signaling, the ecto-5′-NT/NSAP activity ratio and local nucleotide concentrations.

In conclusion, this study provides a robust model for the regulation of two essential signaling molecules for airway defenses, ATP and Ado. The equations capture the complex behavior of the linear and nonlinear reactions and the dynamic

interplay between the ectoenzymes. Furthermore, the model reproduces ASL nucleotide regulation under both static conditions and mechanical stress mimicking normal breathing. Finally, therapeutic applications are proposed based on an interactive approach between simulations and biochemical assays. We are currently developing a model for the regulation of the ASL volume by $P2Y_2$ and A_{2B} receptor-mediated ion channel activities. In the near future, the integration of these two models should provide insightful information on the interactions between the biochemical and functional networks of purinergic signaling on airway epithelia under normal and pathological conditions, as well as novel guidelines for the development of efficient treatments of chronic obstructive lung diseases.

Acknowledgment—We thank Catja van Heusden for technical assistance.

REFERENCES

1. Boucher, R. C. (2003) *Pfluegers Arch.* **445,** 495–498
2. Boucher, R. C. (2007) *J. Int. Med.* **261,** 5–16
3. Davis, C. (2002) *Norvatis Found. Symp.* **248,** 113–125
4. Williams, O. W., Sharafkhaneh, A., Kim, V., Dickey, B. F., and Evans, C. M. (2006) *Am. J. Respir. Cell Mol. Biol.* **34,** 527–536
5. Donaldson, S. H., and Boucher, R. C. (1998) in *The P2 Nucleotide Receptors* (Turner, J. T., Weisman, G. A., and Fedan, J. S., eds) pp. 413–424, Humana Press Inc., Totowa, NJ
6. Marcet, B., and Boeynaems, J. M. (2006) *Pharmacol. Ther.* **112,** 719–732
7. Lazarowski, E. R., Boucher, R. C., and Harden, T. K. (2003) *Mol. Pharmacol.* **64,** 785–795
8. Tarran, R., Button, B., and Boucher, R. C. (2006) *Annu. Rev. Physiol.* **68,** 543–561
9. Kunzelmann, K., Scheidt, K., Scharf, B., Ousingsawat, J., Schreiber, R., Wainwright, B., and McMorran, B. (2006) *FASEB J.* **20,** 545–546
10. Button, B., Picher, M., and Boucher, R. C. (2007) *J. Physiol.* (*Lond.*) **580,** 577–592
11. Guyot, A., and Hanrahan, J. W. (2002) *J. Physiol.* (*Lond.*) **545,** 199–206
12. Lazarowski, E. R., Tarran, R., Grubb, B. R., van Heusden, C. A., Okada, S., and Boucher, R. C. (2004) *J. Biol. Chem.* **279,** 36855–36864
13. Picher, M., Burch, L. H., Hirsh, A. J., Spychala, J., and Boucher, R. C. (2003) *J. Biol. Chem.* **278,** 13468–13479
14. Picher, M., Burch, L. H., and Boucher, R. C. (2004) *J. Biol. Chem.* **279,** 20234–20241
15. Picher, M., and Burch, L. (2006) *Purin. Signal* **2,** 399–408
16. Morse, D. M., Smullen, J. L., and Davis, C. W. (2001) *Am. J. Physiol.* **280,** C1485–C1497
17. Huang, P., Lazarowski, E. R., Tarran, R., Milgram, S. L., Boucher, R. C., and Stutts, M. J. (2001) *Proc. Natl. Acad. Sci. U. S. A.* **98,** 14120–14125
18. Tarran, R., Button, B., Picher, M., Paradiso, A. M., Ribeiro, C. M. P., Lazarowski, E. R., Zhang, L., Collins, P. L., Pickles, R. J., Fredburg, J. J., and Boucher, R. C. (2005) *J. Biol. Chem.* **280,** 35751–35759
19. Boucher, R. C. (2007) *Annu. Rev. Med.* **58,** 157–170
20. Okada, S. F., Nicholas, R. A., Kreda, S. M., Lazarowski, E. R., and Boucher, R. C. (2006) *J. Biol. Chem.* **281,** 22992–23002
21. Takemura, H., Takamura, Y., Isono, K., Tamaoki, J., Nagai, A., and Kawahara, K. (2003) *Jpn. J. Physiol.* **53,** 319–326
22. Zimmermann, H. (2000) *Naunyn-Schmiedeberg's Arch. Pharmacol.* **362,** 299–309
23. Millán, J. (2006) *Purin. Signal* **2,** 335–341
24. Picher, M., and Boucher, R. C. (2000) *Am. J. Respir.* **23,** 255–261
25. Donaldson, S. H., Lazarowski, E. R., Picher, M., Knowles, M. R., Stutts, M. J., and Boucher, R. C. (2000) *Mol. Med.* **6,** 969–982
26. Picher, M., and Boucher, R. C. (2001) *Drug Dev. Res.* **52,** 66–75
27. Donaldson, S. H., Picher, M., and Boucher, R. C. (2002) *Am. J. Respir. Cell Mol. Biol.* **26,** 209–215
28. Picher, M., and Boucher, R. C. (2003) *J. Biol. Chem.* **278,** 11256–11264
29. Hirsh, A. J., Stonebraker, J., van Heusden, C. A., Lazarowski, E. R., Boucher, R. C., and Picher, M. (2007) *Biochemistry* **46,** 10373–10383
30. Fulcher, M. L., Gabriel, S., Burns, K. A., Yankaskas, J. R., and Randell, S. H. (2005) *Methods Mol. Med.* **107,** 183–206
31. Kahner, B. N., Shankar, H., Murugappan, S., Prasad, G. L., and Kunapuli, S. P. (2006) *J. Thromb. Haemost.* **4,** 2317–2326
32. Valero, E., Varon, R., and Garcia-Carmona, F. (2006) *FEBS Lett.* **273,** 3598–3613
33. Dixon, M., and Webb, E. C. (eds) (1979) *Enzymes*, 2nd Ed., 950 pp., Academic Press, New York
34. Christoforidis, S., Papamarcaki, T., Galaris, D., Kellner, R., and Tsolas, O. (1995) *Eur. J. Biochem.* **234,** 66–74
35. Smith, T. M., and Kirley, T. L. (1998) *Biochim. Biophys. Acta* **1386,** 65–78
36. Seargeant, L. E., and Stinson, R. A. (1979) *Can. J. Biochem.* **57,** 2000–2007
37. Pizauro, J. M., Ciancaglini, P., and Leone, F. A. (1993) *Biochim. Biophys. Acta* **1202,** 22–28
38. Demenis, M. A., Furriel, R. P. M., and Leone, F. A. (2003) *Biochim. Biophys. Acta* **1646,** 216–225
39. Knight, G. E., Bodin, P., De Groat, W. C., and Burnstock, G. (2002) *Am. J. Physiol.* **282,** F281–F288
40. Hirschberg, C. B., Robbins, P. W., and Abeijon, C. (1998) *Annu. Rev. Biochem.* **67,** 49–69
41. Bodin, P., and Burnstock, G. (2001) *J. Cardiovasc. Pharmacol.* **38,** 900–908
42. Kreda, S. M., Okada, S. F., van Heusden, C. A., O'Neal, W., Gabriel, S., Abdullah, L., Davis, C. W., Boucher, R. C., and Lazarowski, E. R. (2007) *J. Physiol.* (*Lond.*) **584,** 245–259
43. Adinolfi, E., Pizzirani, C., Idzko, M., Panther, E., Norgauer, J., Di Virgilio, F., and Ferrari, D. (2005) *Purin. Signal* **1,** 219–227
44. Schwiebert, E. M., and Zsembery, A. (2003) *Biochim. Biophys. Acta* **1615,** 7–32
45. Ferrari, D., Pizzirani, C., Adinolfi, E., Lemoli, R. M., Curti, A., Idzko, M., Panther, E., and Di Virgilio, F. (2006) *J. Immunol.* **176,** 3877–3883
46. Eltzschig, H., Weissmüller, T., Mager, A., and Eckle, T. (2006) *Methods Mol. Biol.* **341,** 73–87
47. Spicuzza, L., and Polosa, R. (2003) *Curr. Opin. Allergy Clin. Immunol.* **3,** 65–69
48. Basoglu, O. K., Pelleg, A., Essilfie-Quaye, S., Brindicci, C., Barnes, P. J., and Kharitonov, S. A. (2005) *Chest* **128,** 1905–1909
49. Bennett, W. D., Olivier, K. N., Zeman, K. L., Hohneker, K. W., Boucher, R. C., and Knowles, M. R. (1996) *Am. J. Respir. Crit. Care Med.* **153,** 1796–1801
50. Noone, P. G., Bennett, W. D., Regnis, J. A., Zeman, K. L., Carson, J. L., King, M., Boucher, R. C., and Knowles, M. R. (1999) *Am. J. Respir. Crit. Care Med.* **160,** 144–149
51. Yerxa, B. R., Sabater, J. R., Davis, C. W., Stutts, M. J., Lang-Furr, M., Picher, M., Jones, A. C., Cowlen, M., Dougherty, R., Boyer, J., Abraham, W. M., and Boucher, R. C. (2002) *J. Pharmacol. Exp. Ther.* **302,** 871–880
52. Shaver, S. R., Rideout, J. L., Perdergast, W., Douglass, J. G., Brown, E. G., Boyer, J. L., Patel, R. I., Redick, C. C., Jones, A. C., Picher, M., and Yerxa, B. (2005) *Purin. Signal* **1,** 183–191
53. Munkonda, M. N., Kauffenstein, G., Kukulski, F., Levesque, S. A., Legendre, C., Pelletier, J., Lavoie, E. G., Lecka, J., and Sevigny, J. (2007) *Biochem. Pharmacol.* **74,** 1524–1534
54. Deterding, R., Retsch-Bogart, G., Milgram, L., Gibson, R., Daines, C., Zeitlin, P. L., Milla, C., Marshall, B., Lavange, L., Engels, J., Mathews, D., Gorden, J., Schaberg, A., and Bonnie, W. (2005) *Pediatr. Pulmonol.* **39,** 339–348
55. Sunderman, F. W. (1990) *Ann. Clin. Lab. Sci.* **20,** 123–139
56. Van Belle, H. (1976) *Clin. Chem.* **22,** 972–976
57. Slakey, L. L., Cosimini, K., Earls, J. P., Thomas, C., and Gordon, J. L. (1986) *J. Biol. Chem.* **261,** 15505–15507
58. Pearson, J. D., Carleton, J. S., and Gordon, J. L. (1980) *Biochem. J.* **190,** 421–429
59. Gordon, E. L., Pearson, J. D., and Slakey, L. L. (1986) *J. Biol. Chem.* **261,** 15496–15507
60. Ikehara, Y., Mansho, K., Takahashi, K., and Kato, K. (1978) *J. Biochem.*

(*Tokyo*) **83,** 1471–1483
61. Say, J. C., Ciuffi, K., Furriel, R. P., Ciancaglini, P., and Leone, F. A. (1991) *Biochim. Biophys. Acta* **1074,** 256–262
62. Burnstock, G. (2006) *Novartis Found. Symp.* **276,** 26–48
63. Pankratov, Y., Lalo, U., Verkhratsky, A., and North, R. A. (2006) *Pfluegers Arch.* **452,** 589–597
64. Kukulski, F., Levesque, S. A., Lavoie, E. G., Lecka, J., Bigonnesse, F., Knowles, A. F., Robson, S., Kirley, T. L., and Sevigny, J. (2005) *Purin. Signal* **1,** 193–204
65. Gayle, S., and Burnstock, G. (2005) *Cell Tissue Res.* **319,** 27–36
66. Kim, C. H., Kim, S. S., Choi, J. Y., Shin, J. H., Kim, J. Y., Namkung, W., Lee, J. G., Lee, M. G., and Yoon, J. H. (2004) *Am. J. Physiol.* **287,** L835–L842
67. Taylor, A. L., Schwiebert, L. M., Smith, J. J., King, C., Jones, J. R., Sorscher, E. J., and Schwiebert, E. M. (1999) *J. Clin. Investig.* **104,** 875–884
68. Evans, C. M., Williams, O. W., Tuvim, M. J., Nigam, R., Mixides, G. P., Blackburn, M. R., DeMayo, F. J., Burns, A. R., Smith, C., Reynolds, S. D., Stripp, B. R., and Dickey, B. F. (2004) *Am. J. Respir. Cell Mol. Biol.* **31,** 382–394
69. Vaughan, R. P., Szewczyk, M. T., Lanosa, M. J., DeSesa, C. R., Gianutsos, G., and Morris, J. B. (2006) *Toxicol. Sci.* **93,** 411–421
70. Fabre, A. C., Vantourout, P., Champagne, E., Tercé, F., Rolland, C., Perret, B., Collet, X., Barbaras, R., and Martinez, L. O. (2006) *Cell. Mol. Life Sci.* **63,** 2829–2837
71. Le Hir, M., Gandhi, R., and Dubach, U. C. (1989) *Enzyme* **41,** 87–93
72. Stefanovic, V., Savic, V., Vlahovic, P., Ardaillou, N., and Ardaillou, R. (1988) *Renal Physiol. Biochem.* **11,** 89–102
73. Mitchell, C. H., Carre, D. A., McGlinn, A. M., Stone, R. A., and Civan, M. M. (1998) *Proc. Natl. Acad. Sci. U. S. A.* **95,** 7174–7178
74. Hazama, A., Hayashi, S., and Okada, Y. (1998) *Pfluegers Archiv. Eur. J. Physiol.* **437,** 31–35
75. Hazama, A., Shimizu, T., Ando-Akatsuka, Y., Hayashi, S., Tanaka, S., Maeno, E., and Okada, Y. (1999) *J. Gen. Physiol.* **114,** 525–533
76. Matharu, A.-L., Mundell, S. J., Benovic, J. L., and Kelly, E. (2001) *J. Biol. Chem.* **276,** 30199–30207
77. Mohsenin, A., and Blackburn, M. (2006) *Curr. Opin. Pulm. Med.* **12,** 54–59
78. Gordon, E. L., Pearson, J. D., Dickinson, E. S., Moreau, D., and Slakey, L. L. (1989) *J. Biol. Chem.* **264,** 18986–18995
79. Fadini, G. P., Pauletto, P., Avogaro, A., and Rattazzi, M. (2007) *Atherosclerosis* **193,** 241–244
80. Fleetwood, G., Coade, S. B., Gordon, J. L., and Pearson, J. D. (1989) *Am. J. Physiol.* **256,** H1565–H1572
81. Meghji, P., Pearson, J. D., and Slakey, L. L. (1995) *Biochem. J.* **308,** 725–731
82. Hourani, S. M. (1996) *J. Auton. Pharmacol.* **16,** 349–352